Journal Name RSCPublishing

ARTICLE

Diffusion of Alkali Metals in the First Stage Graphite Intercalation Compounds by vdW-DFT Calculations

Cite this: DOI: 10.1039/x0xx00000x

Received 00th January 2012, Accepted 00th January 2012

DOI: 10.1039/x0xx00000x

www.rsc.org/

Z. Wang[a], A.P. Ratvik[b], T. Grande[a] and S.M. Selbach[a*]

Diffusion of alkali metal cations in the first stage graphite intercalation compounds (GIC) LiC_6, NaC_6, NaC_8 and KC_8 has been investigated with density functional theory (DFT) calculations using the optPBE-vdW van der Waals functional. The formation energies of alkali vacancies, interstitials and Frenkel defects were calculated and vacancies were found to be the dominating point defects. The diffusion coefficients of the alkali metals in GIC were evaluated by a hopping model of point defects where the energy barriers for vacancy diffusion were derived from transition state theory. For LiC_6, NaC_6, NaC_8 and KC_8, respectively, the diffusion coefficients were found to be $1.5\cdot10^{-15}$, $2.8\cdot10^{-12}$, $7.8\cdot10^{-13}$ and $2.0\cdot10^{-10}$ m^2s^{-1} at room temperature, which is within the range of available experimental data. For LiC_6 and NaC_6 a curved vacancy migration path is the most energetically favourable, while a straight pathway was inferred for NaC_8 and KC_8. The diffusion coefficients for alkali metal vacancy diffusion in first stage GICs scales with the graphene interlayer spacing: $LiC_6 << NaC_8 < NaC_6 << KC_8$.

Introduction

Alkali metal graphite intercalation compounds (AM-GICs) display a rich variety of phases with different compositions, which find applications as battery electrodes and in molten salt electrolysis. The Li-GIC system has been intensively studied for decades because of its use in rechargeable lithium ion batteries,[1-8] while Na-GICs are model materials for Na-ion battery anodes.[9-13] Interactions between sodium and graphite is also a key factor in the degradation of cathode lining in aluminium electrolysis cells.[14] In addition, K-GICs have been shown to be superconducting.[15] Diffusion of alkali metals in graphite is imperative to the performance of batteries and the degradation of cathodes linings during aluminium electrolysis. The microscopic mechanisms of diffusion in AM-GICs is however not fully understood due to the lack of reliable theoretical and experimental methods. Quasielastic Neutron Scattering (QENS)[16,17] and nuclear magnetic resonance (NMR)[18] have been used to derive the diffusion coefficients of Li in LiC_6 and K in KC_8. Electrochemical methods, including potentiostatic intermittent titration technique (PITT),[19] galvanostatic intermittent titration technique (GITT)[20] and electrochemical impedance spectroscopy (EIS),[21,22] have also been employed to determine the diffusion coefficient of Li in graphite anode materials. The diffusion coefficient of Na in graphite has been measured by Rapopport test[23] and thermogravimetric analysis of sodium uptake in graphite.[24] The experimentally measured diffusion coefficients are scattered over several orders of magnitude.

Previous density functional theory (DFT) studies of alkali metal diffusion in graphite have primarily focused on Li-GICs, [25-30] while the diffusion of Na in Na-GICs and K in K-GICs has been comparatively less studied and a systematic comparison between Li, Na and K diffusion in GICs is lacking.

Here we study the diffusion of Li, Na and K in first stage graphite intercalation compounds by DFT calculations where the weak van der Waals interactions are accounted for. The optPBE-vdW density functional has recently been shown to accurately describe the structure and energetics of AM-GICs,[31] and this functional was adopted for this study. The energetics of alkali vacancies, interstitials and Frenkel defects in first stage AM-GICs were evaluated and a microscopic diffusion mechanism in AM-GICs was proposed. The energy barriers were calculated according to climbing image Nudged Elastic Band theory[32] and the diffusion coefficients were derived from transition state theory.[25]

Transition state theory

Crystalline materials above 0K contain point defects and these defects are generally mobile and determine the microscopic mechanism and kinetics of solid state mass transport processes. The point defect diffusion coefficient can be obtained from a hopping model using the Einstein-Smoluchowki equation[33]

$$D_{dD} = \frac{a^2}{2d}\Gamma_T \quad (1)$$

where a is the jumping distance, Γ_T the total jumping frequency and d the dimensionality of the diffusion process. Here d is equal to 2 representing a spatially restricted 2D diffusion process. The total jumping frequency is given by equation (2)

$$\Gamma_T = \frac{1}{2}t^{-1} = \frac{1}{2}\left(n_1\omega_1 + n_2\omega_2 + ...\right)^{-1} \quad (2)$$

where t is total jumping time. The factor of 1/2 is due to the success probability of the jump at the intermediate state. n_i is the number of the ith possible elementary jump. ω_i is the ith elementary jump frequency. The total jumping frequency for a curved path in MC_6 and straight path in MC_6 and MC_8 can be derived by equation (3) and (4) respectively, where the details of elementary jumps for each path will be described further below.

$$\Gamma_{T,\mathrm{MC}_6} = \frac{1}{2}\left(\frac{1}{12\omega_1} + \frac{1}{2\omega_2}\right)^{-1} = \frac{6\omega_1\omega_2}{6\omega_1 + \omega_2} \tag{3}$$

$$\Gamma_{T,\mathrm{MC}_8} = \frac{1}{2}\left(\frac{1}{6\omega_1} + \frac{1}{2\omega_2}\right)^{-1} = \frac{3\omega_1\omega_2}{6\omega_1 + \omega_2} \tag{4}$$

The mean jumping frequency, ω_i, can be derived by two approaches. One is based on the Arrhenius equation:

$$\omega_i = \nu_0 \exp\left(-\frac{\Delta E_{h,i}}{k_\mathrm{B} T}\right) \tag{5}$$

where ν_0 denotes the frequency pre-factor which has been often approximated by a constant value in the order of 10^{13} s^{-1},[34] $\Delta E_{h,i}$ is the difference between the energy at an activated state (saddle point) and the initial equilibrium state and k_B is the Boltzmann's constant. Alternatively, the mean jumping frequency can be derived by evaluating the vibrational free energy difference, $\Delta F_{vib,i}$, between an activated state and an initial state, as stated in equation (3)[25]:

$$\omega_i = \frac{k_\mathrm{B}}{T} \exp\left(-\frac{\Delta E_{h,i} + \Delta F_{vib,i}}{k_\mathrm{B} T}\right) \tag{6}$$

where the vibrational free energies are obtained through phonon calculations as described by equation (4) [25]:

$$F_{vib,i} = \sum_j \left(\frac{1}{2} h\nu_j + k_\mathrm{B} T \ln\left[1 - \exp\left(-\frac{h\nu_j}{k_\mathrm{B} T}\right)\right]\right) \tag{7}$$

where ν_j is the vibration frequency of the jth normal mode. Atomic jumping in a diffusion process may consist of several steps and the total jumping frequency is obtained from the individual jumps[25].

Computational details

Density functional theory (DFT) calculations were done with the VASP code,[35-39] using the van der Waals (vdW) functional optPBE-vdW.[40, 41] The optPBE-vdW functional has been carefully evaluated and found to be the most suitable vdW functional for describing the energetics and structural properties of alkali metal graphite intercalation compounds.[31] The projector augmented wave (PAW) method[42] was used with the C_h (2s, 2p), Li_sv (1s, 2s), Na_sv (2s, 2p, 3s) and K_sv (3s, 3p, 4s) potentials supplied with VASP. Electron wave functions were expanded in plane waves up to a cutoff energy of 910 eV and the SCF convergence energy was set to 10^{-7} eV. The high cutoff energy of 910 eV is necessary for vdW DFT calculations to converge with hard carbon potentials, and the C_h potential has previously been found to most accurately describe graphite and higher order GIC.[31] A 2nd order Methfessel-Paxton (MP)[43] smearing of σ = 0.01 eV was used for the electronic energy level occupancy. The Brillouin zone was sampled with a 7 x 7 x 9 Γ-centred k-point mesh for the 2 x 2 x 2 LiC_6 supercell and a similar k-point density was used for other GICs supercells. For the energetics of defect structures the atomic positions were relaxed until the Hellmann-Feynman forces on the ions were smaller than 10^{-3} eV/Å, with the exception of the NaC_6 supercell with a Frenkel defect at the first site and the KC_8 supercell with Frenkel defects at both sites (Figure 1). Relaxation of these three defect structures converged to the corresponding perfect structures, hence static calculations were performed to estimate the defect formation energies. The ground state energies of Li, Na and K metals were done with a 15x15x15 Monkhorst-Pack k-point mesh and with the same convergence criteria as above. Transition state searches were done using the climbing-image nudged elastic band (cNEB)[32] method as implemented in VASP. For all images along the band, atomic positions were relaxed until the Hellmann-Feynman forces on the ions converged to below 0.05 eV/Å with fixed lattice vectors. The frozen phonon method was used to calculate lattice vibrations under the harmonic approximation, as implemented in the Phonopy code.[44] The atomic positions in the supercell were displaced by 0.01 Å in the x, y or z direction to obtain the force constants. Phonon calculations were only performed for first stage LiC_6 supercells with one Li vacancy.

Results

1. Point defect in AM-GICs

Due to the strong chemical bonds within the graphite layers only point defects within the alkali metal layers in the first stage alkali-metal graphite intercalation compounds were considered: alkali vacancies, intersititals and Frenkel defects. The different configurations of these defects in an AM-GIC with MC_6 and MC_8 in-plane superstructures[45] are illustrated in Figure 1. There is one possible vacancy and one possible self-interstitial site, while there are two possible Frenkel sites for each structure. To simulate point defect concentrations of 0.125 and 0.056, 2x2x2 and 3x3x2 supercells were used, respectively.

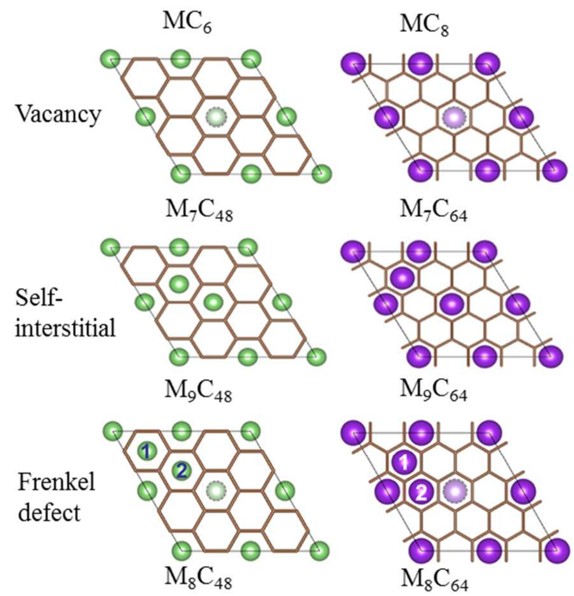

Figure 1. MC_6 and MC_8 supercells with alkali vacancy, self-interstitial and Frenkel defects for an AM-GIC seen along the c-axis. There is one possible vacancy and one possible self-interstitial site, while there are two possible Frenkel sites for each structure.

The defect formation energies were calculated from the change in cohesive energy E_{coh} (binding energy corresponding to sublimation energy) according to Eqs. (5) - (7) for a vacancy, self-interstitial and Frenkel defect, respectively:

$$\Delta E_{f,\mathrm{vac}} = E_{coh,\mathrm{MC_x[vac]}} - E_{coh,\mathrm{MC_x}} + E_{coh,M\ bulk} \tag{8}$$

$$\Delta E_{f,\mathrm{int}} = E_{coh,\mathrm{MC_x[int]}} - E_{coh,\mathrm{MC_x}} - E_{coh,M\ bulk} \tag{9}$$

$$\Delta E_{f,\mathrm{Fre}} = E_{coh,\mathrm{MC_x[Fre]}} - E_{coh,\mathrm{MC_x}} \tag{10}$$

M in MC_x denotes the alkali metal and [vac], [int], [fre] represents vacancy, self-interstitial and Frenkel defect respectively. For example, the internal energy of a vacancy defect in LiC_6 is the energy of a LiC_6 supercell with a vacancy defect minus the energy of a perfect LiC_6 supercell plus the energy of Li metal. The enthalpy of formation for a point defect can be expressed as

$$\Delta H_f = \Delta E_f + pV \approx \Delta E_f \quad (11)$$

since the pV term can be neglected for condensed materials. The calculated defect formation enthalpies in LiC_6, NaC_6, NaC_8 and KC_8 are summarized in Table 1.

Table 1. The calculated defect formation enthalpies for LiC_6, NaC_6, NaC_8 and KC_8 in eV. 2x2x2 supercells were used for NaC_6, NaC_8 and KC_8.

	Vacancy defect	Interstitial defect	Frenkel defect	
			Site 1	Site 2
LiC_6 222	0.166	0.460	0.397	0.651
LiC_6 332	0.175	0.446	0.393	0.635
NaC_6	-0.068	0.946	1.273*	1.210
NaC_8	-0.057	0.882	0.332	0.857
KC_8	0.523	0.561	2.698*	1.381*

*: Relaxation to these three defect structures converged to the corresponding perfect structures, hence static calculations were performed to estimate the defect formation energy.

Vacancies have the lowest defect formation energies for all the first stage AM-GICs and will dominate over interstitials and Frenkel defects. Vacancy diffusion is thus proposed to be the most likely diffusion mechanism in AM-GICs. The negative formation enthalpies for vacancies in NaC_6 and NaC_8 imply that vacancies will form spontaneously. This is in agreement with our previous report: all the first stage Na-GICs are thermodynamically unstable [31].

Defect formation enthalpies were also calculated for both 2x2x2 and 3x3x2 LiC_6 supercells in order to estimate the possible error from the relatively small size of the 2x2x2 supercells. The difference in formation enthalpies between the different supercell sizes were only 0.009-0.016 eV. Increasing the size of the supercell beyond 2x2x2 does not significantly affect the defect formation enthalpies. The following cNEB calculations to study the diffusion of alkali metal in GICs were therefore performed with 2x2x2 supercells due to the excessive computational cost of using larger supercells.

2. Diffusion of alkali metal in the graphite intercalation compounds

2.1 Minimum energy path and diffusion barrier The possible migration pathways for alkali vacancy diffusion in MC_6 and MC_8 structures are illustrated in Figure 2. The migration along the crystallographic c-axis through a hexagonal carbon ring is prohibited due to the high energy barrier.[29,30] The diffusion process in AM-GICs can thus be characterised as 2D diffusion or in-plane diffusion.[27,46] As illustrated in Figure 2b, there are two possible in-plane migration paths in the MC_6 structure: a straight path going over the top of carbon atoms and a curved path travelling over carbon bridges and the hollow of a carbon ring. The distance h in Figure 2b defines the curvature of the curved path. Only one straight migration path is reasonable in the MC_8 structure, as shown in Figure 2c.

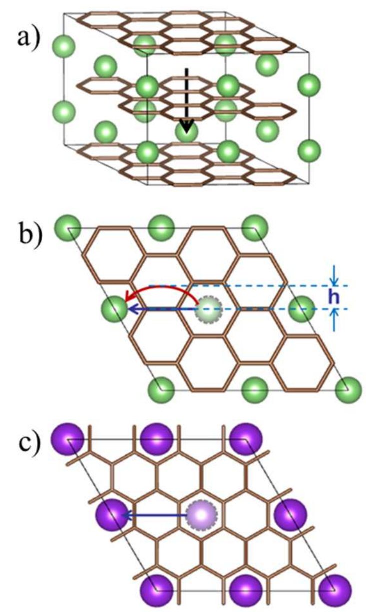

Figure 2. Possible migration paths for vacancy diffusion in (a-b) MC_6 and (c) MC_8 structures. The distance h in Figure 1b defines the curvature of a curved path.

The energetics of the in-plane diffusion pathways for a vacancy defect in LiC_6, NaC_6, NaC_8 and KC_8 are presented in Figure 3 where the relative energies along the proposed diffusion paths are plotted against the distance from the initial vacancy site. The saddle points (transition states) are the highest points along the path. In the MC_6 curved path and the MC_8 straight path the saddle points are the positions where alkali metals are on top of carbon bridges. In the MC_6 straight path the saddle points are the positions of alkali metal on top of carbon atoms. There are two saddle point along the paths in all the structures, E_1 and E_2 denote the two corresponding energy barriers, where E_1 is the energy difference between the saddle point and the initial state and E_2 is the energy difference between the saddle point and the intermediate state at the middle point along the diffusion pathway.

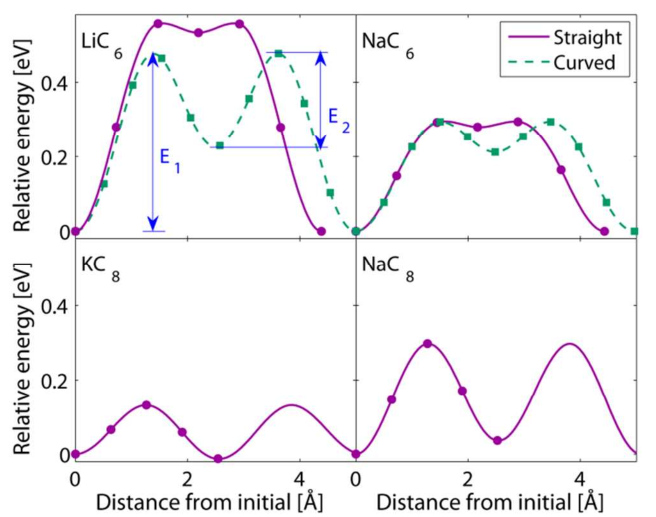

Figure 3. Relative energies along the in-plane diffusion pathways for vacancy defects in LiC_6, NaC_6, NaC_8 and KC_8. The points are the calculated values (images) while the lines are spline fitting curves.

The energies of the initial and final states are identical and set to 0 as a reference. E_1 and E_2 in the figures represent the energy differences between the saddle points and initial states and intermediate points, respectively. Due to symmetry, only one half of the pathways in the MC_8 structures were calculated.

The energy barriers E_1 and E_2 and the relative energies of the saddle and intermediate points for vacancy diffusion pathways in LiC_6, NaC_6, NaC_8 and KC_8 are summarized in Table 2.

Table 2. Energy barriers of a vacancy defect in LiC_6, NaC_6, NaC_8 and KC_8 structure, unit in [eV].

		LiC_6	NaC_6	NaC_8	KC_8
Straight	Saddle	0.57	0.30	0.30	0.13
	Intermediate	0.53	0.28	0.04	-0.01
	E_1	0.57	0.30	0.30	0.13
	E_2	0.04	0.02	0.26	0.14
Curved	Saddle	0.48	0.29	NA	NA
	Intermediate	0.23	0.21	NA	NA
	E_1	0.48	0.29	NA	NA
	E_2	0.25	0.08	NA	NA

The cNEB calculations show that the energy barrier for the first jump (E_1) is always higher than for the second jump (E_2), meaning that the first jump is the rate limiting step in the diffusion process. For diffusion in LiC_6 and NaC_6 the path with the lowest energy barriers is the minimum energy path (MEP). For LiC_6 the energy at the saddle point for the straight path is 0.09 eV higher than along the curved path. For NaC_6, this energy difference is only 0.01 eV.

The calculated energy profile for LiC_6 along the curved path in Figure 3 is similar to the LDA (local density approximation) calculated by Toyura *et al*.[25]. As the concentration of alkali metal in a GIC increases with lower stage numbers Li-C interactions become progressively more important compared to vdW forces. This is why first stage GIC like LiC_6 can be described relatively well by conventional LDA or PBE GGA. For higher stage GICs vdW interactions will dominate progressively with increasing stage number and the use of vdW functionals is imperative.[31] For consistency and comparison with higher stage GIC vdW functionals were also used in the present work on first stage GIC.

2.2 Jumping frequency and diffusion coefficient The two energy barriers along the diffusion pathways imply that the diffusion process consists of two steps. As illustrated in Figure 4, the first jump is from the initial site to the intermediate site, with 12 possible elementary jumps along a curved path, and with 6 possible jumps along a straight path. The second step is from the intermediate site to another vacancy site from which 2 possible elementary jumps exist.

The diffusion coefficients were derived by evaluating the mean jumping frequency for each step and finally the total jumping frequency. Arrhenius plots of the diffusion coefficients of Li, Na and K in the first stage graphite intercalation compounds are shown in Figure 5. The curved diffusion pathway was chosen for Li in LiC_6 and Na in NaC_6 since it leads to a higher diffusion coefficient compared to the straight pathway, which will be discussed further below. Experimental diffusivity data[16-24] are included for comparison.

In general, the calculated diffusivities are in good agreement with the data acquired by Quasielastic Neutron Scattering (QENS)[16,17] and Nuclear magnetic resonance (NMR).[18] The data from electrochemical methods, as for the case of LiC_6, including

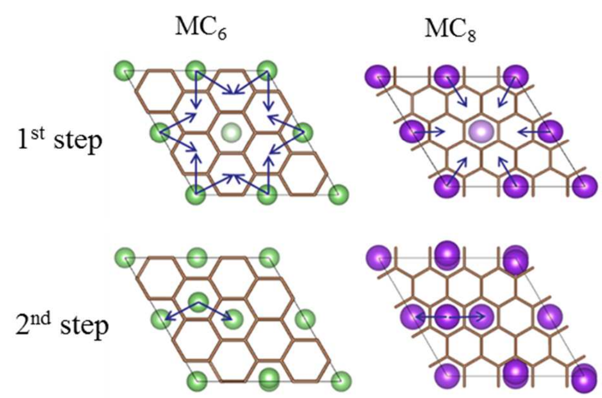

Figure 4. Possible elementary jumps for alkali metal atoms from an initial site to a vacancy site (final state) for (a) curved pathway and (b) straight pathway.

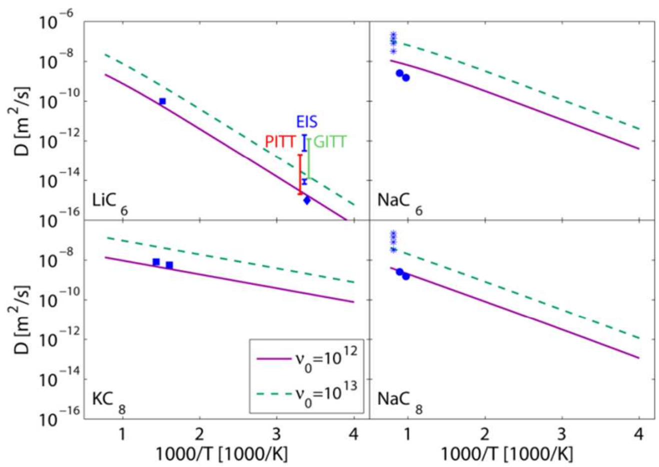

Figure 5. Calculated Arrhenius plots of vacancy defect diffusivity in first stage LiC_6, NaC_6, NaC_8 and KC_8. The results for LiC_6 and NaC_6 are calculated from curved diffusion pathways, while those for NaC_8 and KC_8 are from straight pathways. The points are experimental results from different methods: "*": Rapopport test[23], "●": Na thermo-gravimetric test,[24] "■": QENS,[16,17] "♦": NMR.[18] The error bars show the data measured by electrochemical methods including PITT,[19] GITT[20] and EIS.[21,22] All the electrochemical data were measured at room temperature. The positions of the error bars are shifted to improve the readability.

potentiostatic intermittent titration technique (PITT),[19] galvanostatic intermittent titration technique (GITT)[20] and electrochemical impedance spectroscopy (EIS),[21,22] are scattered over a relatively large range from $1.2\cdot10^{-15}$ to $1.7\cdot10^{-12}$ m^2/s. The data from electrochemical methods are scafttered because the measurements cover a wide range of the state of charge (SOC): the concentration of Li in graphite varies during the measurements. The calculated diffusivities for NaC_6 and NaC_8 are also in good agreement with the measurements from Rapopport test[23] and Na thermo-gravimetric test.[24] However, deviations for NaC_6 and NaC_8 are also expected since these two compounds are thermodynamically unstable.[31] The real Na concentration in graphite is expected to be considerable lower, corresponding to a higher stage number.[47]

The activation energy (E_a) of a diffusion process can be determined from an Arrhenius plot according to equation (9)

$$D = D_0 \exp\left(-\frac{E_a}{k_B T}\right) \quad (12)$$

where D_0 is a pre-exponential factor. The diffusion coefficients D of Li, Na and K in graphite intercalation compounds at 25 °C and 960 °C, the activation energies (E_a) and the pre-exponential factors (D_0) are summarized in Table 3. The calculated activation energies are within the value range of the available experimental data.

Discussion

The diffusion coefficients in Table 3 were derived by the Arrhenius approach according to Equation (1) and (5), where the empirical vibration pre-factor (v_0) was set to 10^{12} and 10^{13}, respectively,[34] giving diffusion coefficients within a range of one order of magnitude. The contribution from changes in the vibrational free energy, however, can also be elucidated through phonon calculations according to Equation (6) and (7). These two methods are compared in Figure 6. It is clear that within the calculated temperature range, the results from the phonon calculations lie between the results from the Arrhenius approach with the two empirical vibration pre-factors. At room temperature, the line with v_0 equal to 10^{12} is closer to the quantum statistics' result, while at elevated temperatures the line with v_0 equal to 10^{13} is closer. In general, the Arrhenius approach gives good estimates for the diffusion coefficients in the considered structures. Taking into consideration the scattered experimental data, computationally heavy phonon calculations would not provide additional insight. From the steeper slope in Figure 6 it is clear that the activation energy inferred from quantum statistics is slightly higher than that from the Arrhenius approach; 0.50 eV and 0.48 eV, respectively.

Table 3. Diffusion coefficients D at 25 °C and 960 °C, activation energies (E_a) and pre-exponential factors (D_0) for LiC_6, NaC_6, NaC_8 and KC_8. Experimental data for activation energies are included for comparison.

	LiC_6	NaC_6	NaC_8	KC_8
D @ 25 °C [m^2/s]	$1.5 \cdot 10^{-15}$	$2.8 \cdot 10^{-12}$	$7.8 \cdot 10^{-13}$	$2.0 \cdot 10^{-10}$
D @ 960 °C [m^2/s]	$1.8 \cdot 10^{-9}$	$1.0 \cdot 10^{-8}$	$3.6 \cdot 10^{-9}$	$1.3 \cdot 10^{-8}$
Activation energy [eV]	0.47	0.28	0.28	0.14
D_0	$2.29 \cdot 10^{-7}$	$2.10 \cdot 10^{-7}$	$5.24 \cdot 10^{-8}$	$4.68 \cdot 10^{-8}$
Activation energy Ex. [eV]	0.55 [18] 1.0 [16] 0.2 [48]	NA	NA	0.18 [17]

1. Curved vs. straight diffusion path in MC_6 structures

The diffusion coefficients of Li and Na in LiC_6 and NaC_6 obtained from straight and curved paths (Figure 2) are listed in Table 4. The diffusion along a curved path is faster than along a straight path for both compounds, with a difference of more than one order of magnitude for Li in LiC_6 and a factor of three for Na in NaC_6. It is evident that the curved path is the minimum energy path (MEP) in both structures.

The curved path does not pass exactly at the middle of the carbon ring, but is pushed towards the straight path due to the repulsive forces between adjacent alkali metal ions. The curvature can be quantified as h as illustrated in Figure 2b. The lower the value of h the closer the curved path is to the straight path. The curvature h in Table 4 demonstrates that Li travels along a more curved path with h equal to 1.20 Å while Na follows a more straight path with h equal to 0.99 Å. The larger Na ions give rise to stronger repulsive forces than the smaller Li ions do. Consequently, a smaller difference in the diffusion coefficient between a curved and a straight path is found for Na in the NaC_6 structure.

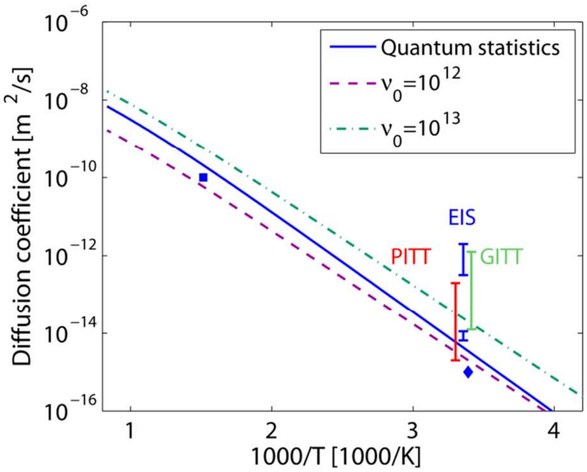

Figure 6. Vacancy defect diffusivity in LiC_6 structure as a function of inverse temperature. The solid line is calculated from quantum statistics; the dashed and dash-dotted lines are based on Arrhenius approach with pre-factors v_0 equal to 10^{12} and 10^{13}, respectively. Experimental data are also included for comparison with the same notations as in Figure 5.

Table 4. Diffusion coefficients for vacancy diffusion at 25 °C for LiC_6 and NaC_6 structures. v_0 in equation (2) is set to 10^{12}.

	LiC_6	NaC_6
Straight	$3.2 \cdot 10^{-17}$ [m^2/s]	$9.5 \cdot 10^{-13}$ [m^2/s]
Curved	$1.5 \cdot 10^{-15}$ [m^2/s]	$2.8 \cdot 10^{-12}$ [m^2/s]
h	1.20 Å	0.99 Å

2. Charge transfer and redistribution during vacancy migration

As demonstrated in our previous work, in GIC the valence s electron of alkali metal atoms are donated to carbon p_z orbitals where the electrons are delocalized.[31] Alkali metal vacancies cause a redistribution of charge around the vacancy site and the charge density difference between the LiC_6 supercell with and without a Li vacancy is illustrated in Figure 7a. The charge density difference along the central line in the graphene layer is shown in Figure 7b. Compared to the total charge density this difference is subtle.

The diffusion of alkali metal ions in AM-GICs leads to a redistribution of charge around the moving ions. The redistribution of electrons close to the Fermi energy indicates how the chemical bonding is affected by the elementary jumps. The partial charge density difference between the initial state and the saddle point for Li in LiC_6 and K in KC_8 are shown in Figure 8a and 8b, respectively. Only electrons with energy within the range of E_F-2eV to E_F were considered. The linear partial charge density differences for the graphene layer between the initial and saddle points are illustrated for LiC_6, KC_8, NaC_6 and NaC_8 in Figure 8c-8f, respectively.

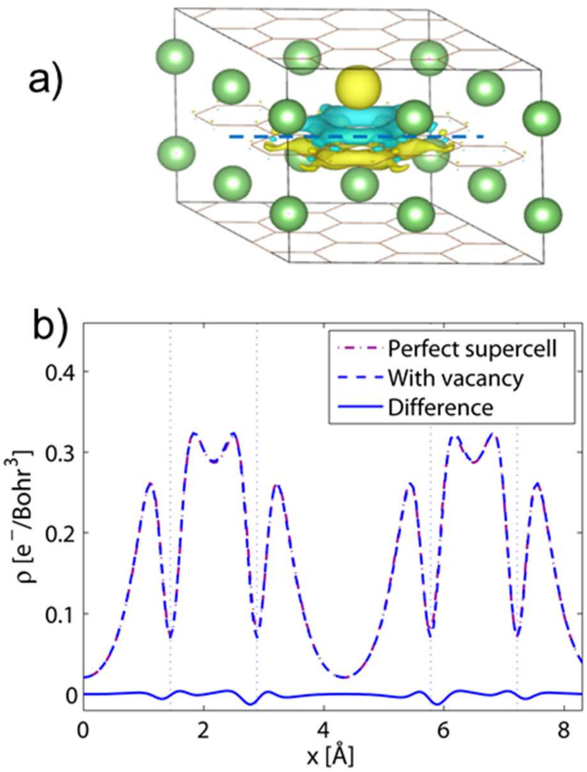

Figure 7. (a) Charge density (ρ) between the LiC_6 perfect supercell and the supercell with a Li vacancy. Isosurface levels were set to be +0.01 $e^-/Bohr^3$ (yellow) and -0.01 $e^-/Bohr^3$ (blue). (b) Charge density (ρ) along the line in figure 7a through the graphene layer.

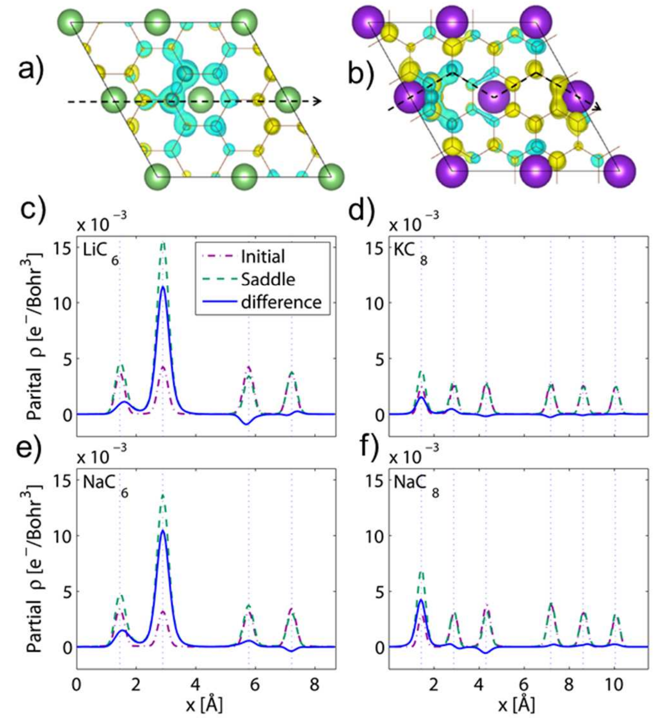

Figure 8. Partial charge density difference between a (a) LiC_6 and (b) KC_8 supercell with a vacancy at the initial site and at the saddle point. Only the electrons with the energy within the region of E_F - 2eV to E_F were considered. Isosurface levels were set to ±0.0013 $e^-/Bohr^3$ for LiC_6 and ±0.0003 $e^-/Bohr^3$ for KC_8 where yellow is positive and blue is negative. Partial charge density through the graphene layer for a vacancy travelling along the line in Figure 1(a) and (b) in (c) LiC_6, (d) KC_8, (e) NaC_6 and (f) NaC_8.

Compared to the small difference in partial charge density for a stationary vacancy in Figure 7, a substantial partial charge density difference for an AM atom at the initial site and a saddle point is evident from Figure 8. The electrons with energies from E_F-2 eV to E_F can be exclusively designated to C 2p_z orbitals [31] which form a π^* band with delocalized electrons. The high mobility of the C 2p_z electrons close to E_F allows a substantial charge redistribution in the graphene layer when an AM ion migrates. The partial charge density differences in the graphene layer is smaller for the MC_8 crystal structure where the carbon coordination number is lower. The relative partial charge density differences between LiC_6 and NaC_6, and between NaC_8 and KC_8, reflect the different graphene interlayer distances.

From a structural point of view, the calculated diffusion coefficients of Li, Na and K in the first stage GICs correlate with the graphene inter-layer distance, as illustrated in Figure 9. The largest ion, K^+, gives the largest separation of the adjacent graphene layers and the highest diffusion coefficient. In Na-GICs, the interlayer distances are subtly larger in NaC_6 than in NaC_8 and the diffusion of Na in NaC_6 is slightly faster in NaC_6 than in NaC_8. The diffusivities in AM-GICs follow the sequence: $KC_8 >> NaC_6 > NaC_8 >> LiC_6$. The diffusion coefficients decrease with increasing activation energy and diffusion energy barrier (E_1), which corresponds to the first elementary jump of the diffusion process.

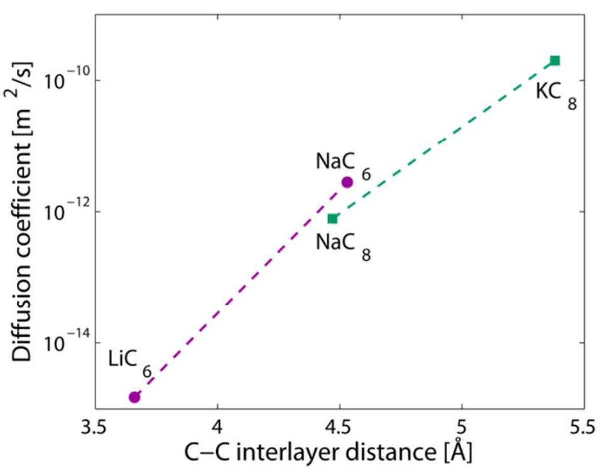

Figure 9. Diffusion coefficients (at 25 °C, v_0 equal to 10^{12}) for alkali metal vacancy diffusion as a function of graphene interlayer spacing.

Real carbon materials like graphite or amorphous carbon contain grain boundaries, surfaces and other imperfections. Although the energy barriers for diffusion can differ from crystalline bulk in amorphous carbon and in the vicinity of structural defects, the crystalline GIC studied in this work is the ideal model system for real carbon materials used in batteries and electrodes.

Conclusion

Alkali metal vacancies were shown to be the dominating type of point defects in first stage alkali metal intercalation compounds GIC) from van der Waals density functional theory calculations. Diffusion of alkali metals in first stage GIC is thus inferred to occur through the diffusion of vacancies. In LiC_6 and NaC_6 a curved migration path parallel to carbon bridges in adjacent graphene layers was found to be the most energetically favourable migration pathway. A straight path crossing the carbon bridges in adjacent graphene layers is the most favourable migration pathway in NaC_8 and KC_8. The calculated diffusion coefficients are within the range of experimentally found values. The diffusivities of alkali metals in GIC were shown to be strongly correlated with the graphene inter-layer spacing, and scale as follows: $KC_8 >> NaC_6 > NaC_8 >> LiC_6$.

Acknowledgements

The present work was carried out in the project Durable Materials in Primary Aluminium Production (DuraMat), financed by the research Council of Norway, Hydro Primary Aluminum Technology, Sør-Norge Aluminium (Søral), and Elkem Carbon. Permission to publish the results is gratefully acknowledged. Computational resources were provided by NOTUR (The Norwegian Metacentre for Computational Science) through the projects nn2962k, nn9268k and nn9264k.

Notes and references

[a] Department of Materials Science and Engineering, Norwegian, University of Science and Technology, NO-7491Trondheim, Norway.
[b] SINTEF Materials and Chemistry, NO-7465 Trondheim, Norway.
[c] Corresponding author: selbach@material.ntnu.no

1. R. Yazami and P. Touzain, *J. Power Sources*, 1983, 9, 365-371.
2. N. Takami, A. Satoh, M. Hara and I. Ohsaki, *Journal of The Electrochemical Society*, 1995, 142, 371-379.
3. A. Mabuchi, K. Tokumitsu, H. Fujimoto and T. Kasuh, *J. Electrochem. Soc.*, 1995, **142**, 1041-1046.
4. J. B. Goodenough, *J. Solid State Electrochem.*, 2012, **16**, 2019-2029.
5. J. S. Filhol, C. Combelles, R. Yazami and M. L. Doublet, *J. Phys. Chem. C*, 2008, **112**, 3982-3988.
6. J. Sangster, *J. Phase Equilib. Diffus.*, 2007, **28**, 561-570.
7. M. Winter, J. O. Besenhard, M. E. Spahr and P. Novak, *Adv. Mater.*, 1998, **10**, 725-763.
8. M. Endo, C. Kim, K. Nishimura, T. Fujino and K. Miyashita, *Carbon*, 2000, **38**, 183-197.
9. Y. L. Cao, L. F. Xiao, W. Wang, D. W. Choi, Z. M. Nie, J. G. Yu, L. V. Saraf, Z. G. Yang and J. Liu, *Adv. Mater.*, 2011, **23**, 3155-+.
10. R. Alcantara, P. Lavela, G. F. Ortiz and J. L. Tirado, *Electrochem. Solid State Lett.*, 2005, **8**, A222-A225.
11. S. W. Kim, D. H. Seo, X. H. Ma, G. Ceder and K. Kang, *Adv. Energy Mater.*, 2012, **2**, 710-721.
12. D. A. Stevens and J. R. Dahn, *J. Electrochem. Soc.*, 2000, **147**, 1271-1273.
13. M. D. Slater, D. Kim, E. Lee and C. S. Johnson, *Adv. Funct. Mater.*, 2013, **23**, 947-958.
14. K. Tschöpe, A. Støre, A. Solheim, E. Skybakmoen, T. Grande and A. Ratvik, *JOM*, 2013, **65**, 1403-1410.
15. R. A. Jishi and M. S. Dresselhaus, *Phys. Rev. B*, 1992, **45**, 12465-12469.
16. A. Magerl, H. Zabel and I. S. Anderson, *Phys. Rev. Lett.*, 1985, **55**, 222-225.
17. H. Zabel, A. Magerl, J. J. Rush and M. E. Misenheimer, *Phys. Rev. B*, 1989, **40**, 7616-7632.
18. J. Langer, V. Epp, P. Heitjans, F. A. Mautner and M. Wilkening, *Phys. Rev. B*, 2013, **88**, 094304.
19. M. D. Levi and D. Aurbach, *J. Phys. Chem. B*, 1997, **101**, 4641-4647.
20. H. Yang, H. J. Bang and J. Prakash, *J. Electrochem. Soc.*, 2004, **151**, A1247-A1250.
21. N. Takami, A. Satoh, M. Hara and T. Ohsaki, *J. Electrochem. Soc.*, 1995, **142**, 371-379.
22. P. Yu, B. N. Popov, J. A. Ritter and R. E. White, *J. Electrochem. Soc.*, 1999, **146**, 8-14.
23. A. P. Ratvik, A. Støre, A. Solheim and T. Foosnæs, *Light Metals (TMS) 2014*, **2008**, 973-978.
24. Z. Wang, A. P. Ratvik, E. Skybakmoen and T. Grande, *Light Metals (TMS) 2014*, **2014**, 1239-1244.
25. K. Toyoura, Y. Koyama, A. Kuwabara, F. Oba and I. Tanaka, *Phys. Rev. B*, 2008, **78**, 214303.
26. K. Toyoura, Y. Koyama, A. Kuwabara and I. Tanaka, *J. Phys. Chem. C*, 2010, **114**, 2375-2379.
27. K. Persson, V. A. Sethuraman, L. J. Hardwick, Y. Hinuma, Y. S. Meng, A. van der Ven, V. Srinivasan, R. Kostecki and G. Ceder, *J. Phys. Chem. Lett.*, 2010, **1**, 1176-1180.
28. K. Persson, Y. Hinuma, Y. S. Meng, A. Van der Ven and G. Ceder, *Phys. Rev. B*, 2010, **82**, 125416.
29. V. Meunier, J. Kephart, C. Roland and J. Bernholc, *Phys. Rev. Lett.*, 2002, **88**, 075506.
30. S. Thinius, M. M. Islam, P. Heitjans and T. Bredow, *J. Phys. Chem. C*, 2014, **118**, 2273-2280.
31. Z. Wang, S. M. Selbach and T. Grande, *RSC Adv.*, 2014, **4**, 4069-4079.
32. G. Henkelman, B. P. Uberuaga and H. Jónsson, *J. Chem. Phys.*, 2000, **113**, 9901-9904.
33. H. Mehrer, *Diffusion in Solids*, Springer, 2006.
34. A. Van der Ven, G. Ceder, M. Asta and P. D. Tepesch, *Phys. Rev. B*, 2001, **64**, 184307.
35. P. E. Blöchl, *Phys. Rev. B*, 1994, **50**, 17953-17979.
36. G. Kresse and J. Hafner, *Phys. Rev. B*, 1993, **47**, 558-561.
37. G. Kresse and J. Hafner, *Phys. Rev. B*, 1994, **49**, 14251-14269.
38. G. Kresse and J. Furthmüller, *Comput. Mater. Sci.*, 1996, **6**, 15-50.
39. G. Kresse and J. Furthmüller, *Phys. Rev. B*, 1996, **54**, 11169-11186.
40. M. Dion, H. Rydberg, E. Schröder, D. C. Langreth and B. I. Lundqvist, *Phys. Rev. Lett.*, 2004, **92**, 246401.
41. G. Román-Pérez and J. M. Soler, *Phys. Rev. Lett.*, 2009, **103**, 096102.
42. G. Kresse and D. Joubert, *Phys. Rev. B*, 1999, **59**, 18.
43. M. Methfessel and A. T. Paxton, *Phys. Rev. B*, 1989, **40**, 3616-3621.
44. A. Togo, F. Oba and I. Tanaka, *Phys. Rev. B*, 2008, **78**, 134106.
45. M. S. Dresselhaus and G. Dresselhaus, *Adv. Phys.*, 2002, **51**, 1-186.
46. H. Zabel and S. A. Solin, eds., *Graphite Intercalation Compounds I*, Springer-Verlag Berlin Heidelberg, Germany, 1990.
47. R. C. Asher and S. A. Wilson, *Nature*, 1958, **181**, 409-410.
48. H. Estrade, J. Conard, P. Lauginie, P. Heitjans, F. Fujara, W. Buttler, G. Kiese, H. Ackermann and D. Guérard, *Physica B+C*, 1980, **99**, 531-535.